Available online at www.sciencedirect.com
SCIENCE DIRECT
Surface Science 600 (2006) 703–715
SURFACE SCIENCE
www.elsevier.com/locate/susc

Converged properties of clean metal surfaces by all-electron first-principles calculations

Juarez L.F. Da Silva [a,*], Catherine Stampfl [a,b], Matthias Scheffler [a]

[a] Fritz-Haber-Institut der Max-Planck-Gesellschaft, Faradayweg 4-6, D-14195 Berlin-Dahlem, Germany
[b] The School of Physics, The University of Sydney, Sydney 2006, Australia

Received 25 January 2005; accepted for publication 1 December 2005
Available online 28 December 2005

Abstract

All-electron full-potential linearized augmented plane-wave calculations of the surface energy, work function, and interlayer spacings of close-packed metal surfaces are presented, in particular, for the free-electron-like metal surfaces, Mg(0 0 0 1) and Al(1 1 1), and for the transition metal surfaces, Ti(0 0 0 1), Cu(1 1 1), Pd(1 1 1), and Pt(1 1 1). We investigate the convergence of the surface energy as a function of the number of layers in the slab, using the Cu(1 1 1) surface as an example. The results show that the surface energy, as obtained using total energies of the slab and bulk from separate calculations, converges well with respect to the number of layers in the slab. Obviously, it is necessary that bulk and surface calculations are performed with the same high accuracy. Furthermore, we discuss the performance of the local-density and generalized gradient approximations for the exchange–correlation functional in describing the various surface properties.

Keywords: Density functional theory calculations; Low index single crystal surfaces; Surface energy; Surface relaxation; Work function; Copper; Aluminum; Palladium; Platinum

1. Introduction

The surface energy, work function, and interlayer spacings of metal surfaces are important physical properties which play a role in determining the behavior of solid metal surfaces when used in various applications, for example, heterogeneous catalysis, electrochemistry, corrosion, lubrication, etc. [1,2]. The surface energy of the various crystallographic facets determine the equilibrium shape of crystals, however, the direct experimental measurements of the surface energy are difficult to perform and subject to various uncertainties, e.g., presence of impurities. In addition, most of the available experimental surface-energy data of metals are obtained from surface tension measurements in the liquid phase and extrapolated to zero temperature [3,4], which does not provide the orientation dependence of the surface energy. Due to the difficulties in obtaining experimental surface energies, as well as their orientation dependence [5,6], accurate calculations based on modern first-principles methods play an important role [7–11].

There are two approaches by which to obtain surface energies from first-principles calculations: (i) one may evaluate the total energy of a slab of the particular solid and subtract the corresponding bulk total energy obtained from a separate calculation. Alternatively, (ii), one may use slabs of different thicknesses and extract from them the energy of a bulk atom. Boettger et al. [12,13] and Fiorentini and Methfessel [14] argued that approach (i) is problematic, yielding surface energies that diverge linearly as a function of the slab thickness. The origin of this problem is that

* Corresponding author. Present address: Humboldt-Universitaet zu Berlin, Institut fuer Chemie, Arbeitsgruppe Quantenchemie, Unter den Linden 6, D-10099 Berlin, Germany. Tel.: +49 3020937140; fax: +49 3020937136.
E-mail address: dasilvaj@chemie.hu-berlin.de (J.L.F. Da Silva).
URL: http://www.geocities.com/dasilva_juarez/ (J.L.F. Da Silva).

0039-6028/$ - see front matter © 2005 Elsevier B.V. All rights reserved.
doi:10.1016/j.susc.2005.12.008

often slab and bulk total energies are calculated with different levels of accuracy. Thus, Fiorentini and Methfessel suggested that approach (ii) is superior: extracting the bulk total energy from the slope of the slab total energy versus the number of layers in the slab ensures that surface and bulk are extracted with the same accuracy. We will show below, however, that well converged surface energies can be obtained from separate bulk and slab calculations, provided that slab and bulk systems are calculated with the same high accuracy.

The work function is the minimum energy required for an electron to escape from a solid through a certain surface and it is orientation dependent. In particular, the work function changes are an important source of information in the study of adparticles on surfaces [2]. Adsorbates that have higher electronegativities than the substrate atoms typically increase the work function, while those with lower electronegativities have the opposite effect. For example, Na atoms adsorbed on Al(1 1 1) decrease the substrate work function by a large amount, i.e., ≈1.40 eV at coverage 1/3 of a monolayer (ML) [2]. The electronegativity of Na is 0.93 and that of Al is 1.61, thus there is displacement of electron density from Na toward the substrate, which gives rise to an adsorbate-induced surface dipole. An opposite effect is observed for Cl adsorbed on Al(1 1 1) where there is charge transfer from the substrate to Cl, so that Cl is partially negatively charged and sits on an adsorption site which is positively charged [2]. The adsorption of rare-gas atoms on metal surfaces also induce a decrease in the substrate work function, e.g., Xe on Pt(1 1 1) for coverage 1/3 ML, reduces the work function by 1.36 eV. For these systems, the mechanism is due to an adsorbate-induced polarization of adparticle and substrate surface [15–17]. In many cases, experimental values of the work function are only available for *polycrystalline* materials [18,19]. Thus, first-principles calculations are valuable in order to predict work functions, or even better, work function *differences* for different surface crystallographic orientations.

Experimentally, the best accessible surface property is the atomic structure, i.e., the interlayer relaxations. The atomic structure can be obtained with high accuracy using quantitative low-energy electron diffraction (LEED) intensity analysis [20–33]. And theoretically, first-principles calculations also give an accurate description, see for example, Refs. [7,34–53], where it has been found that the majority of transition metal surfaces show a contraction of the first interlayer spacing, i.e., the spacing between the two outermost layers is smaller than in the bulk terminated (unrelaxed) surface. An expansion of the outermost interlayer spacing has been reported, e.g., for Mg(0 0 0 1) [29,33,37,44,45], Al(1 1 1) [11,22,24,28,31,46], and Pt(1 1 1) [21,22,47,50].

In the present paper we employ the all-electron full-potential linearized augmented plane-wave (FP-LAPW) method for the study of the following problems: (i) Convergence of the surface energy with slab thickness using the close-packed Cu(1 1 1) surface as an example. The interlayer spacings and work function as a function of the thickness of the slab will be also discussed. (ii) Performance of the local-density approximation and the generalized gradient approximation in the study of the surface properties using, as an example, two free-electron-like metal surfaces, i.e., Mg(0 0 0 1) and Al(1 1 1), and four transition metal surfaces, i.e., Ti(0 0 0 1), Cu(1 1 1), Pd(1 1 1), and Pt(1 1 1). (iii) In the literature, one occasionally finds that calculated surface properties are still obtained at the experimental lattice constant, instead of the equilibrium theoretical value. Thus, it is interesting to see how the surface properties of metal surfaces differ when obtained at experimental and theoretical lattice constants. (iv) Due to the high accuracy of the FP-LAPW method, our well converged results may serve as a benchmark with which to compare the results of other computational approaches, e.g., semi-empirical calculations.

This paper is organized as follows: In Section 2, the theoretical approach and computational details are described. In Section 3, we present and discuss the bulk and surface properties, as well as comparison with other theoretical and experimental results. Section 4 summarizes the main conclusions, while Appendix A lists the total energies used to calculate the surface energies of Cu(1 1 1) for different slab thickness, and discusses the affect of the broadening parameter of the Fermi–Dirac distribution function on the surface properties.

2. Theoretical approach and computational details

All calculations are performed using density functional theory (DFT) [54,55] with the local-density approximation (LDA) [56,57] and the generalized gradient approximation (GGA) to describe the exchange–correlation energy functional. For the GGA functional, we use the formulation proposed by Perdew et al. [58], which is commonly called PBE. The Kohn–Sham equations are solved using the all-electron FP-LAPW method [59], as implemented in the WIEN code [60–62]. This implementation includes total energy and atomic force calculations, which allows a structural optimization via a damped molecular-dynamics approach [63].

The core states are treated fully relativistically, while the semi-core and valence states are treated by the scalar relativistic approximation, i.e., spin–orbit coupling is included (neglected) for the core (semi-core and valence) states. The FP-LAPW wave functions in the interstitial region are represented using a plane-wave expansion truncated to include only plane waves that have kinetic energies less than some particular cutoff energy, E^{wf}, and for the potential representation in the interstitial region, plane waves with kinetic energies up to E^{pot} are considered. Inside the muffin-tin spheres with radius R_{mt}, the wave functions are expanded in radial functions (solution of the radial Schrödinger equation) times spherical harmonics up to $l_{\mathrm{max}}^{\mathrm{wf}}$, and for the representation of the potential inside the muffin-tin spheres, a maximum of $l_{\mathrm{max}}^{\mathrm{pot}}$ is used. In the present work:

$E^{wf} = 12.5$ Ry (Mg and Ti), 14.1 Ry (Al and Pd), and 16.7 Ry (Cu and Pt); $R_{mt} = 1.27$ Å (Mg, Ti, Al, and Pd) and 1.16 Å (Cu and Pt). $l^{wf}_{max} = 12$ (Mg, Al, and Ti) and 10 (Cu, Pd, and Pt); $E^{pot} = 144$ Ry (LDA) and 169–256 Ry (PBE); $l^{pot}_{max} = 6$ for all systems.

The integration of the Brillouin zones (BZ) is performed using the special **k**-point method [64] where the broadening of the Fermi surface is done using the Fermi-function with an artificial electronic temperature of 0.05 eV (given as $k_B T_{el}$) [65,66]. The BZ integrations for the bulk calculations are performed using $(12 \times 12 \times 12)$ and $(16 \times 16 \times 10)$ Monkhorst–Pack grids for face-centered cubic (fcc) and hexagonal close-packed (hcp) structures, respectively. From systematic LDA calculations of the surface energies of the unrelaxed Cu(1 1 1) surface as a function of the number of **k**-points in the irreducible part of the BZ (see surface energy section), we found that well converged surface energies can be obtained using a $(16 \times 16 \times 1)$ Monkhorst–Pack grid in the (1×1) surface unit cell, which correspond to 30 **k**-points in the irreducible part of the BZ.

The close-packed metal surfaces are modeled using a (1×1) surface unit cell consisting of a finite number of layers separated by a vacuum region of 15 Å. For the Al(1 1 1), Cu(1 1 1), Pd(1 1 1), and Pt(1 1 1) surfaces seven layers were used, while eight layers were used for the Mg(0 0 0 1) and Ti(0 0 0 1) surfaces. Both sides of the slab are relaxed and it is assumed that the surface atoms are in the equilibrium configuration when the force on each atom is smaller than 0.70 mRy/bohr. The convergence of bulk and surface properties with respect to the number of **k**-points and cutoff energy have been carefully tested and are reported in Ref. [15].

3. Results and discussion

3.1. Bulk properties

Total energy calculations are performed for 13 regularly spaced volumes, which are obtained by varying the volume within ±3.0% of the experimental volume. The volumes at zero pressure (equilibrium volume), bulk moduli calculated at the equilibrium volume, and the cohesive energies are obtained using Murnaghan's equation of state [67]. Furthermore, for comparison, the bulk moduli and cohesive energies are also calculated at the experimental volumes [67]. Calculation of the cohesive energy requires the total energy of the free atoms, which are obtained from spin-polarized calculations using a cubic box with side length of 10.58 Å and one **k**-point, $\left(\frac{1}{4},\frac{1}{4},\frac{1}{4}\right)\frac{2\pi}{a}$, in the irreducible part of the BZ.[1] In this way the total energy of the bulk and free atom systems are both calculated at the same level of approach for the core and valence states, i.e., inclusion of spin–orbit coupling only for the core states. All our results are obtained at zero temperature and no corrections are made for the zero point energy. The bulk cohesive properties calculated with the LDA and PBE functionals, as well as experimental results and other ab initio results, are summarized in Table 1. The errors in percent with respect to the experimental results [68] are also given.

We find that the LDA underestimates the lattice constant for all studied systems, while the PBE overestimates it for Cu, Pd, and Pt. For Mg, Al, and Ti, the PBE also underestimates it, but only by a small amount, i.e., <0.50%. Considering the relative errors with respect to the experimental values, the PBE provides a better description for Mg, Al, Ti, and Cu, while for Pt, the LDA performs better. For Pd, the relative error obtained with the LDA and PBE are almost the same, but in opposite directions. The bulk moduli show a corresponding trend to that obtained for the equilibrium lattice constant (i.e., an overestimate for lattice constants that are underestimated), however, the relative errors in the bulk moduli are significantly larger compared to those of the equilibrium lattice constants.

With regard to the cohesive energy, the LDA overestimates it for *all* systems, which is the usual finding [69,70]. The largest error occurs for Ti (38.14%) and the smallest for Mg (16.56%). The PBE underestimates the cohesive energy for Mg, Pd, and Pt, while it overestimates it for Al, Ti, and Cu. In general, the PBE provides a better overall agreement with experimental results, as the relative errors compared to the experimental results are smaller, as can be seen from inspection of Table 1.

We find good agreement with the results of other ab initio calculations [11,37–39,41,46,51,69–72]; however, in some particular cases there are deviations. For example, for Mg we find that the magnitude of our LDA cohesive energy (equilibrium lattice constant) differs by +0.33 eV (−0.08 Å) compared to the value obtained by Fuchs et al. [69] using the pseudopotential plane wave (PPPW) method. Furthermore, we obtain that $c_0/a_0 = 1.623$ (LDA) and 1.620 (PBE), while Fuchs et al. [69] reported 1.59 (LDA) and 1.66 (PBE); the experimental one is 1.62. These differences might be due to the frozen core approximation that is the basis of the pseudopotential approach. We note that for bulk Al, we obtain good agreement with the PPPW calculations of Fuchs et al. [69] and FP-LAPW calculations of Da Silva [11]. The equilibrium lattice constant and bulk moduli for Al, Cu, and Pt are very close to those reported by Khein et al. [71] (cf. Table 1), in which the FP-LAPW method was also used. Cohesive energies were not reported in Ref. [71].

We find that the cohesive energies calculated using the experimental volume differ very little (see Table 1); the greatest deviation being 0.05 eV for Ti with the LDA. Correspondingly, Ti exhibits the greatest deviation (−2.71%) to the experimental lattice constant of all the elements studied. The bulk moduli, however, are significantly more sensitive to deviations in the volume, which is explained due

[1] We found in earlier work [70] that the *k*-point, $\left(\frac{1}{4},\frac{1}{4},\frac{1}{4}\right)\frac{2\pi}{a}$, yielded faster convergence of the total energy with cell size as compared to selecting the Γ-point.

Table 1
Bulk cohesive properties of Mg, Al, Ti, Cu, Pd, and Pt

Bulk		a_0 (Å)		B_0 (Mbar)			E_{coh} (eV)		
Mg	LDA[a]	3.13 $c_0/a_0 = 1.623$	−2.49%	0.38	+8.57%	(0.28; −20.00%)	−1.77	+17.22%	(−1.75; +15.89%)
	PBE[a]	3.20 $c_0/a_0 = 1.620$	−0.31%	0.34	−2.86%	(0.33; −5.71%)	−1.50	−0.66%	(−1.50; −0.66%)
	LDA	3.05[b], 3.12[c]		0.39[b], 0.38[c]			−2.09[b]		
	GGA	3.20[b]		0.30[b]			−1.42[b]		
	Exp.[d]	3.21 $c_0/a_0 = 1.624$		0.35			−1.51		
Al	LDA[a]	3.98	−1.73%	0.84	+16.67%	(0.47; −34.72%)	−4.07	+20.06%	(−4.06; +19.76%)
	PBE[a]	4.04	−0.25%	0.78	+8.33%	(0.75; +4.17%)	−3.60	+6.19%	(−3.60; +6.19%)
	LDA	3.97[e], 3.98[f]		0.80[e], 0.84[f]			−4.09[e]		
	PBE	4.04[g]		0.75[g]			−3.65[g]		
	GGA	4.05[e], 4.04[h]		0.73[e], 0.71[h]			−3.54[e]		
	GGA	4.05[b], 4.09[f]		0.79[b], 0.73[f]			−3.52[b]		
	Exp.[d]	4.05		0.72			−3.39		
Ti	LDA[a]	2.87 $c_0/a_0 = 1.577$	−2.71%	1.26	+20.00%	(0.92; −12.38%)	−6.70	+38.14%	(−6.65; +37.11%)
	PBE[a]	2.94 $c_0/a_0 = 1.579$	−0.34%	1.12	+6.67%	(1.06; +0.95%)	−5.87	+21.03%	(−5.87; +21.03%)
	LDA	2.88[i], 2.93[j]		1.32[j]					(−6.29[k])
	Exp.[d]	2.95 $c_0/a_0 = 1.588$		1.05			−4.85		
Cu	LDA[a]	3.52	−2.49%	1.92	+40.15%	(1.26; −8.03%)	−4.57	+30.95%	(−4.53; +29.80%)
	PBE[a]	3.63	+0.55%	1.42	+3.65%	(1.54; +12.41%)	−3.51	+0.57%	(−3.51; +0.57%)
	LDA	3.55[b]		1.72[b]			−4.31[b]		
	LDA	3.52[f]		1.92[f]			−4.29[k]		
	PBE	3.63[l]		1.38[l]			−3.74[l]		
	GGA	3.67[b]		1.34[b]			−3.38[b]		
	GGA	3.62[f]		1.51[f]			−3.30[k]		
	Exp.[d]	3.61		1.37			−3.49		
Pd	LDA[a]	3.85	−1.03%	2.22	+22.65%	(1.87; +3.31%)	−5.04	+29.60%	(−5.03; +29.31%)
	PBE[a]	3.95	+1.54%	1.63	−9.94%	(2.10; +16.02%)	−3.63	−6.68%	(−3.62; −6.94%)
	LDA	3.88[m]		2.25[m]			−5.05[m]		
	Exp.[d]	3.89		1.81			−3.89		
Pt	LDA[a]	3.89	−0.77%	3.05	+9.71%	(2.66; +8.13%)	−7.16	+22.60%	(−7.15; +16.71%)
	PBE[a]	3.97	+1.28%	2.41	−13.31%	(2.96; +6.47%)	−5.59	−4.28%	(−5.57; −4.62%)
	LDA	3.90[f]		3.07[f]					
	GGA	3.97[f]		2.46[f]					
	Exp.[d]	3.92		2.78			−5.84		

Equilibrium lattice constant, a_0, bulk modulus, B_0, and cohesive energy, E_{coh}. The numbers in parentheses are the values calculated using the experimental lattice constants. The relative error with respect to the experimental value is given in percent.

[a] Present work using the FP-LAPW method.
[b] PPPW method, Ref. [69].
[c] PPPW method, ($c_0/a_0 = 1.616$), Ref. [37].
[d] Experimental result, Ref. [68].
[e] PPPW method, Ref. [70].
[f] LAPW method, Ref. [71].
[g] FP-LAPW method, Ref. [11].
[h] PPPW method, Ref. [46].
[i] LAPW method, ($c_0/a_0 = 1.581$), Ref. [39].
[j] PPPW method, ($c_0/a_0 = 1.594$), Ref. [41].
[k] Slater-Type Orbitals (STOs), Ref. [72]; (expt. geometry).
[l] FP-LAPW method, Ref. [51].
[m] PPPW method, Ref. [38].

the linear dependence of the bulk modulus with respect to the pressure [67]. For example, for Ti, as calculated with the LDA, it varies from being +20.00% greater than experiment (1.05 Mbar) with a value of 1.26 Mbar at the

theoretical equilibrium volume, to being −12.38% less, with a value of 0.92 Mbar when the experimental value is used. Another large variation occurs for Al, as obtained using the LDA: at the theoretical volume the bulk modulus is 0.84 Mbar (+16.67% larger than experiment, which is 0.72 Mbar), while using the experimental value (which is 1.73% greater), the bulk modulus is 0.47 Mbar, significantly (−34.72%) less than experiment. Bulk moduli calculated with the PBE functional, in general, exhibit less dramatic changes to those obtained using the experimental volume since the theoretical lattice constant is closer to the experimental one.

3.2. Clean surface properties

To test the convergence of the surface properties with number of layers in the slab, N_l, we consider the variation of the surface energy, work function, and interlayer spacings of the Cu(1 1 1) surface as a function of N_l. We consider $N_l = 1$ up to 12. All layers in the slab are allowed to relax.

3.2.1. Surface energy

The surface energy is the energy (per surface atom or per unit area) needed to split an infinite crystal into two semi-infinite crystals. Then, conceptually, it is straightforward to calculate the surface energy using this definition. The surface energy per surface atom is given by

$$\sigma = \frac{1}{2}\left(E_{\text{tot}}^{\text{slab}} - N_l E_{\text{tot}}^{\text{bulk}}\right), \tag{1}$$

where $E_{\text{tot}}^{\text{slab}}$ is the total energy of a slab with N_l layers (one atom per atomic layer) and $E_{\text{tot}}^{\text{bulk}}$ is the reference total energy per atom of the bulk system. The factor $\frac{1}{2}$ takes into account that there are two equivalent surfaces in the slab. $E_{\text{tot}}^{\text{bulk}}$ may be calculated from a separate bulk calculation, or it may be determined from the expression,

$$E_{\text{tot}}^{\text{bulk}} = E_{\text{tot}}^{\text{slab}}(N_l + 1) - E_{\text{tot}}^{\text{slab}}(N_l) = \partial E_{\text{tot}}^{\text{slab}}(N)/\partial N \tag{2}$$

provided that N_l is large enough. This is so since two slabs of different thickness, $N_l + 1$ and N_l, only differ by one bulk layer.

As a first test, we calculated the surface energy of the seven-layer unrelaxed Cu(1 1 1) surface using the LDA functional and employing Eq. (1) as a function of the number of **k**-points. For these calculations, the slab and bulk total energies were calculated using $(n \times n \times 1)$ and $(n \times n \times n)$ Monkhorst–Pack grids [64], respectively. The results are plotted in Fig. 1. We found that for $n = 8$, 10, 12, 14, 16, 18, 20, 22, 24, 26, and 28 the surface energies differ by 59.6, 48.8, 4.4, 9.2, 2.2, 2.4, 3.9, 2.9, 0.2, 3.3, and 1.2 meV, respectively, to the converged value obtained for $n = 30$.

Because earlier work [12,14] had argued that the surface energy, as defined in Eq. (1), may diverge as a function of N_l when $E_{\text{tot}}^{\text{bulk}}$ is obtained from a separate bulk calculation, we evaluate the reference bulk total energy using three different approaches: (i) calculated separately with the same (or similar) quality **k**-point mesh as the slab calculation; (ii) calculated separately with a better quality **k**-point mesh than the slab calculation; (iii) using a linear fit to $E_{\text{tot}}^{\text{slab}}(N_l)$ with $N_l = 3, \ldots, 12$. For these calculations the total energies of the Cu(1 1 1) slabs are obtained using an $(8 \times 8 \times 1)$ **k**-point set, yielding 10 **k**-points in the irreducible part of the surface Brillouin zone. The resulting surface energies are shown in Fig. 2.

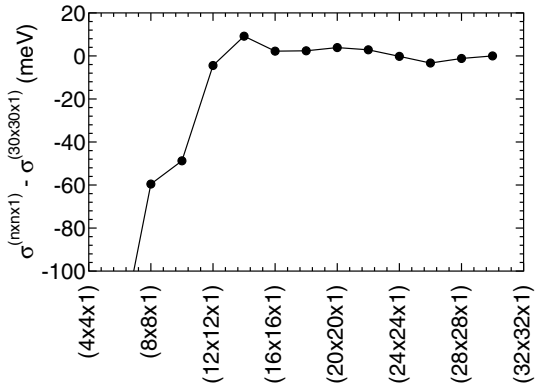

Fig. 1. Relative convergence of the surface energy of the seven-layer unrelaxed Cu(1 1 1) surface calculated with the LDA as a function of increasing **k**-point mesh size. The slab and the bulk were calculated using $(n \times n \times 1)$ and $(n \times n \times n)$ Monkhorst–Pack grids, respectively.

Fig. 2 shows clearly that the surface energy obtained using approach (i) (squares) with **k**-meshes of $(8 \times 8 \times 1)$

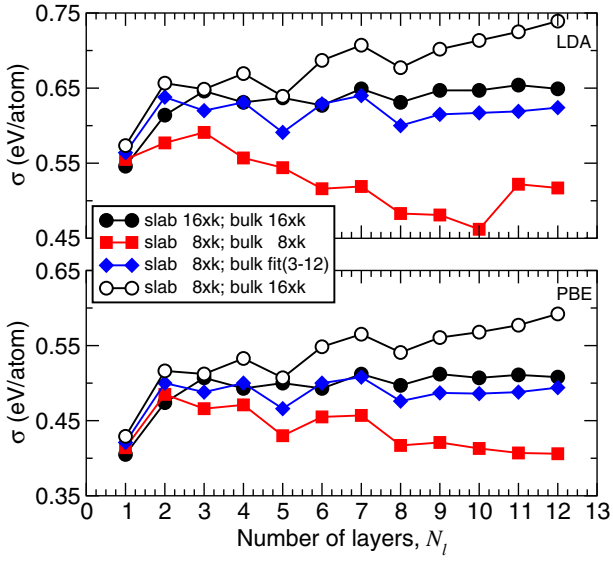

Fig. 2. Surface energy, σ, of the Cu(1 1 1) surface as a function of the number of layers in the slab, N_l. The squares correspond to surface energies calculated using bulk total energies obtained with a similar quality **k**-point set $(8 \times 8 \times 8)$ as the slab calculation $(8 \times 8 \times 1)$, the open circles for surface energies obtained using a higher quality **k**-point set for the bulk calculation $(16 \times 16 \times 16)$ as compared to the surface $(8 \times 8 \times 1)$, and diamonds for surface energies obtained using the bulk total energy determined from a fit to a series of slab total energies calculated using a **k**-point mesh of $(8 \times 8 \times 1)$. The closed circles indicate surface energies calculated using a larger **k**-point set (namely, $16 \times 16 \times 1$) for the slab and a similar quality mesh for the bulk total energy (i.e., $16 \times 16 \times 16$). In these calculations the theoretical equilibrium lattice constant is used.

and $(8\times8\times8)$ for the slab and bulk, respectively, decreases with increasing slab thickness. This problem is not improved by approach (ii) (open circles), in which the slabs and bulk are calculated with a $(8\times8\times1)$ and $(16\times16\times16)$ MP grid, respectively. In this case the surface energy also diverges, but in the opposite direction. Using method (iii) (diamonds) i.e., obtaining the bulk total energy by a fit to a series of slab total energies calculated with the $(8\times8\times1)$ MP grid, the surface energy nicely converges with increasing slab thickness.

We also calculated the surface energy using a larger **k**-point set (namely, $16\times16\times1$, corresponding to 30 in the IBZ) and a similar quality mesh for the bulk energy (i.e., $16\times16\times16$). The result is plotted in Fig. 2 (closed circles). It can be seen that the values are very similar to those obtained by approach (iii). Thus, performing separate total energy calculations for the slabs and bulk systems *does not* lead to surface energies which diverge with respect to the number of layers in the slab, *providing* that each system is calculated with sufficiently high accuracy. Very similar behavior is obtained using the LDA and PBE functionals. The total energies of the slabs calculated with the two different **k**-point sets are listed in Table 4.

To obtain a deeper understanding of the dependence of the surface energy as a function of the slab thickness, we compared our results for Cu(1 1 1) with similar calculations performed by Da Silva for Al(1 1 1), also using the FP-LAPW method [11]. The results reported in Fig. 3 indicate similar behavior for both systems, however, larger oscillations are observed for the Al(1 1 1) surface. Therefore, our results indicate a smaller dependence of the surface energy of Cu(1 1 1) as a function of the slab thickness compared with systems like Al(1 1 1). For example, it can be seen in Figs. 2 and 3 that around three or four layers (for Cu(1 1 1)) provide well converged surface energies, e.g., $\sigma(12\text{ L})-\sigma(3\text{ L})=3.0$ meV (LDA). Nevertheless, other properties are not well converged with so few layers; for example, the interlayer spacings require six or more layers (see below). Given this, we therefore use seven layers to calculate the surface properties of the Al(1 1 1), Pd(1 1 1), and Pt(1 1 1) surfaces, while eight layers are used for Mg(0 0 0 1) and Ti(0 0 0 1) surfaces.

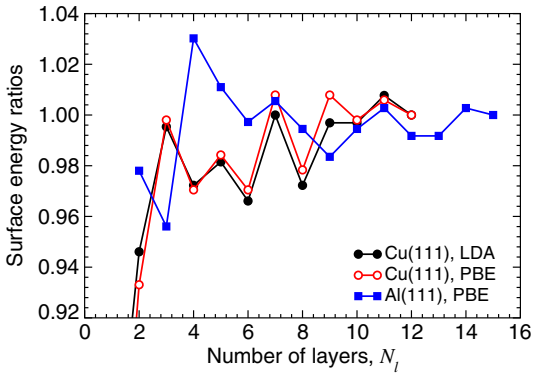

Fig. 3. Surface energy ratios, $\sigma^{\star}$, for the Cu(1 1 1) and Al(1 1 1) surfaces as a function of the number of layers in the slab. $\sigma^{\star}=\sigma(N_l)/\sigma(N_l=12)$ for Cu(1 1 1) and $\sigma(N_l)/\sigma(N_l=15)$ for Al(1 1 1).

The surface energies obtained using the LDA and PBE functionals, and the theoretical as well as the experimental lattice constants, are summarized in Table 2, along with earlier published theoretical results. For all studied cases the PBE functional predicts a smaller surface energy compared to the LDA, e.g., for Cu(1 1 1) $\sigma=0.64$ eV/atom (LDA) and 0.50 eV/atom (PBE), which is the same as the trend obtained for the cohesive energies. Similar trend, i.e., $\sigma^{\mathrm{PBE}}<\sigma^{\mathrm{LDA}}$, was also obtained by Yu and Scheffler [10] for the low-Miller-index Pb surfaces.

We found that for Ti(0 0 0 1) and Cu(1 1 1), the experimental result lies between the LDA and PBE values, and for the other systems, the LDA results are closer to experiment. For the case of Pt(1 1 1), in which the LDA result is closer to experiment, we checked the dependence of the surface energy on the spin–orbit interaction for the valence states. By including the spin–orbit interaction also for the valence states, we obtained a surface energy of 0.84 eV/atom for Pt(1 1 1), which is 0.07 eV/atom smaller compared to the result without taking into account the spin–orbit interaction for the valence states. This result is in accord with the all-electron calculations reported in Ref. [50], which obtained that spin–orbit coupling decreases the surface energy of the Pt(1 1 1) surface by 0.20 eV/atom.

From our results, it seems that the LDA gives better values for the surface energies than the PBE functional. The latter gives surface energies about 30% lower than the experimental values. The apparently better performance of the LDA (in this respect) is probably due to a better error cancellation of the surface exchange and correlation energy within the LDA [57]. It is important to point out that the experimental surface energies reported in Table 2 are obtained from surface tension measurements in the liquid phase and extrapolated to zero temperature. Hence the value represents an average surface energy over a large number of surface terminations. Thus, any direct comparison between our calculated surface energies and the experimental results to access the performance of the LDA and PBE functionals should be taken with caution.

We also calculated the surface energies using the experimental lattice constant. The experimental lattice constant was used for both the bulk and slab calculations. The results are summarized in Table 2. It can be seen that the values are very similar to those obtained using the theoretical lattice constant, however, there are some deviations: For example, results using the experimental lattice constant are 5.90% for Ti(0 0 0 1) (LDA), 6.25% for Cu(1 1 1) (LDA), 7.10% for Pd(1 1 1) (PBE), and 14.10% for Pt(1 1 1) (PBE) lower compared to those obtained using the theoretical equilibrium lattice constant.

The values reported by Vitos et al. [9] using the tight-binding linear-muffin-tin orbitals (TB-LMTO) approach with the atomic sphere approximation (ASA) are considerably larger than our all-electron PBE values for all studied systems, e.g., larger by 0.3 eV/atom for Ti(0 0 0 1). The

Table 2
Surface energy, σ, and work function, Φ, of the Mg(0001), Al(111), Ti(0001), Cu(111), Pd(111), and Pt(111) surfaces

		Mg(0001)	Al(111)	Ti(0001)	Cu(111)	Pd(111)	Pt(111)
σ (eV/atom)	LDA[a]	0.33 (0.33)	0.39 (0.39)	1.01 (0.95)	0.64 (0.60)	0.75 (0.76)	0.91 (0.93)
	PBE[a]	0.31 (0.30)	0.33 (0.34)	0.93 (0.93)	0.50 (0.51)	0.56 (0.51)	0.71 (0.61)
	LDA	0.36[b]	0.56[b]	0.90[b]	0.69[b]	0.68[c]	0.98[b]
	LDA			1.04[d]		0.77[b], 0.75[e]	1.10[f]
	GGA	0.44[g]	0.53[g], 0.36[h]	1.23[g]	0.71[g]	0.82[g]	1.00[g], 0.85[f]
σ (J/m^2)	LDA[a]	0.62 (0.59)	0.91 (0.88)	2.27 (2.02)	1.92 (1.69)	1.87 (1.86)	2.23 (2.24)
	PBE[a]	0.56 (0.54)	0.75 (0.77)	1.99 (1.98)	1.41 (1.44)	1.33 (1.25)	1.67 (1.47)
	LDA	0.64[b]	0.83[i]	2.19[j]	1.94[i]	1.64[c]	2.35[b]
	LDA		1.27[b]	1.95[b], 2.24[d]	1.96[b], 1.59[k]	1.88[b]	
	GGA	0.79[g], 0.64[l]	1.20[g], 0.82[h]	2.63[g]	1.95[g]	1.92[g]	2.30[g]
	Exp.	0.79[m]	1.14[m]	2.10[n]	1.83[n]	2.01[n]	2.49[m]
	Exp.		1.16[n]	1.99[m]	1.79[m]	2.00[m]	2.48[n]
Φ (eV)	LDA[a]	3.80 (3.83)	4.21 (4.19)	4.66 (4.54)	5.22 (5.03)	5.64 (5.63)	6.06 (6.04)
	PBE[a]	3.65 (3.65)	4.04 (4.04)	4.40 (4.38)	4.78 (4.82)	5.22 (5.26)	5.69 (5.73)
	LDA	3.86[b]	4.17[i], 4.54[b]	4.64[j], 4.59[b]	5.10[i], 5.30[b]	5.53[c], 5.90[b]	6.74[b]
	LDA			4.75[d]	5.19[k]		6.53[f]
	GGA		4.09[o], 4.06[h]				
	Exp.	3.66[n]	4.48[p], 4.24[n]	4.33[n]	4.94[n], 4.90[p]	5.95[p], 5.55[q]	6.40[p], 5.85[p]
	Exp.					5.44[r]	6.10[s]

The numbers in parentheses were calculated using the experimental lattice constant (for both the slab and the bulk), instead of the theoretical equilibrium lattice constant.
[a] Present work using the FP-LAPW method.
[b] TB-LMTO–ASA method, Ref. [8]
[c] FP-LMTO method, Ref. [7].
[d] PPPW method, Ref. [41].
[e] PPPW method, Ref. [38].
[f] FP-LAPW method, Ref. [50].
[g] TB-LMTO–ASA method, Ref. [9].
[h] FP-LAPW method, Ref. [11].
[i] FP-LMTO method, Ref. [36].
[j] LAPW method, Ref. [39].
[k] PPPW method, Ref. [35].
[l] PPPW method, Ref. [37].
[m] Experimental result, Ref. [3].
[n] Experimental result, Ref. [4].
[o] PPPW method, Ref. [46].
[p] Experimental result, Ref. [19].
[q] Experimental result, Ref. [74].
[r] Experimental result, Ref. [75].
[s] Experimental result, Ref. [73].

reason for this may be due to the ASA approximation, which does not allow for sufficient flexibility of electronic relaxation at the surface. Furthermore, Skriver and Rosengaard [8] using the TB-LMTO–ASA method reported surface energies calculated with the LDA using the experimental lattice constant. They are in reasonable agreement with our results, but again often exhibiting a slightly larger value as for the results of Vitos et al. The largest deviation being for Al(111) where they obtained 0.56 eV/atom compared to our 0.39 eV/atom, while our value is very close to the result obtained by Da Silva [11] of 0.36 eV/atom.

3.2.2. Work function

The work function, Φ, of a solid surface is the minimum energy required to remove an electron from the surface, and is given by

$$\Phi = V_{es}(\mathbf{r}_{vac}) - E_F, \quad (3)$$

where E_F is the Fermi energy of the system and $V_{es}(\mathbf{r}_{vac})$ is the electrostatic potential far from the surface, which is chosen to be in the middle of the vacuum region of the slab. We calculate the work function of the Cu(111) surface as a function of the number of layers in the slab. The results obtained with the LDA and PBE functionals are plotted in Fig. 4. For layers greater than about four, the values deviate only by small amounts and may be regarded as being converged. Thus, quantum size effects are apparently small in this system, though some indication (e.g., minima at $N_l = 7$ and 10 are present). The work functions for all the surfaces are summarized in Table 2 along with experimental and previous theoretical results.

The LDA functional predicts larger work functions than the PBE functional for all studied surfaces, e.g., $\Phi^{LDA} - \Phi^{PBE} = 0.15$ eV and 0.44 eV for Mg(0001) and Cu(111), respectively. Inspecting the results in Table 2 we see that

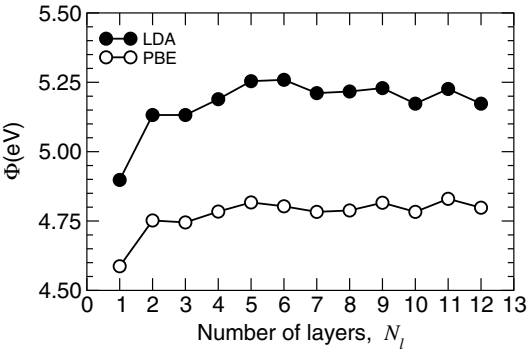

Fig. 4. Work function, Φ, of the Cu(1 1 1) surface as a function of the numbers of layers in the slab, N_l. All layers are allowed to relax. In these calculations the theoretical equilibrium lattice constant is used.

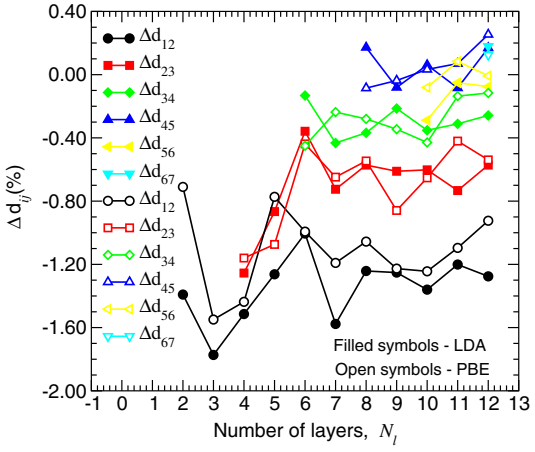

Fig. 5. Interlayer spacings, $\Delta d_{ij} = 100(d_{ij} - d_0)/d_0$, of the Cu(1 1 1) surface as a function of the number of layers in the slab, N_l. All layers were allowed to relax. In these calculations the theoretical equilibrium lattice constant is used. d_0 is given by $a_0/\sqrt{3}$.

for Mg(0 0 0 1), the PBE yields close agreement with experiment (3.66 eV compared to 3.65 eV (PBE)). However, this apparent agreement may be incidental since the experimental work function is for polycrystalline Mg. For Al(1 1 1), the experimental results (4.48 and 4.24 eV) are closer to the LDA results. For Ti(0 0 0 1), similarly to Mg(0 0 0 1), the PBE (4.40 eV) yields closer agreement to the experimental value (4.33 eV), however again the experimental work function is for polycrystalline material.

With regard to the Cu(1 1 1) surface, the experimental results lie roughly in between the LDA and PBE values. For Pd(1 1 1), the differences between the LDA and PBE values are smaller than the differences between the experimental results (5.44, 5.55, and 5.95 eV), hence, it is difficult to establish any conclusion concerning the performance of the LDA and PBE for this particular case. For Pt(1 1 1), the experimental results (5.85, 6.10, and 6.40 eV) also exhibit a significant deviation from each other. It becomes clear that further accurate experimental measurements of work functions would be valuable and necessary for more quantitative comparison with theory. The values of the work functions obtained using the experimental lattice constant are quite similar to those obtained using the theoretical one. The two largest deviations are for the Ti(0 0 0 1) and Cu(1 1 1) systems using the LDA, where the values obtained using the experimental lattice constant are 2.6% and 3.6% less than those obtained using the theoretical one.

In general our results for the work function are in good agreement with previous theoretical calculations for all studied systems, except for Pt(1 1 1), in which a work function of 6.74 eV was obtained using the LDA in Ref. [8] with the TB-LMTO–ASA method, while our result is 6.06 eV. Such difference might be due to the TB and ASA approximations.

3.2.3. Interlayer spacing relaxations

The creation of a surface alters the electron density of the topmost surface layers, and hence the atoms change their atomic positions. Fig. 5 shows the surface relaxations for Cu(1 1 1) calculated with the LDA and PBE functionals as a function of the number of layers in the slab. The changes in the interlayer spacings are presented with respect to the unrelaxed interlayer spacing, i.e., $\Delta d_{ij} = 100(d_{ij} - d_0)/d_0$, where d_0 is $a_0/\sqrt{3}$ for fcc(1 1 1) and $c_0^h/2$ for hcp(0 0 0 1). It can be seen from Fig. 5 that a larger number of layers in the slab, i.e., 7, are required to obtain converged interlayer relaxations compared to the surface energy and work function. The interlayer relaxations for all studied surfaces calculated using seven and eight layers for the fcc(1 1 1) and hcp(0 0 0 1) surfaces, respectively, are summarized in Table 3 along with LEED and previous theoretical results.

For all studied surfaces, the LDA and PBE functionals predict very similar results (see Table 3). Thus, the agreement between quantitative LEED analyses and DFT calculations does not depend critically on the exchange–correlation functional employed. However, the LDA and PBE predict quite different interlayer relaxations when the *experimental* lattice constant is used (see Table 3). Even qualitatively different relaxations are obtained using the experimental lattice constant. For example, for Pd(1 1 1), the LDA predicts a contraction of −2.20% for the topmost interlayer spacing, while the PBE predicts an expansion of +2.94%. However, using the respective LDA and PBE theoretical lattice constants, both functionals predict very similar results [−0.22% (LDA) and −0.01% (PBE)]. Similar result was found by Feibelman and Hamann for the Rh(0 0 1) surface employing also the LAPW method [34], however, in their work was restricted to the topmost interlayer relaxation. The reason for this behavior is due to the strain imposed by performing the calculations at the experimental value. For Cu(1 1 1) the experimental lattice constant is 2.50% larger than that obtained theoretically with the LDA. This results in the greater interlayer contractions when the experimental lattice constant is used (−6.33% versus −1.58%) because the atoms relax to try and roughly preserve the theoretical equilibrium volume. Compared to the value obtained with the PBE functional, the experimental

Table 3
Changes in the interlayer spacings, Δd_{ij}, of closed-packed metal surfaces calculated with the LDA and PBE functionals

		Mg(0001)	Al(111)	Ti(0001)	Cu(111)	Pd(111)	Pt(111)
Δd_{12}	LDA[a]	+1.18 (−2.59)	+1.35 (−2.08)	−6.44 (−11.32)	−1.58 (−6.33)	−0.22 (−2.20)	+0.88 (−0.82)
(%)	PBE[b]	+1.24 (+0.91)	+1.35 (+1.09)	−6.84 (−8.00)	−1.19 (−0.44)	−0.01 (+2.94)	+1.14 (+3.98)
	LDA	+1.13[b], +1.50[c]		−7.70[d]	−1.27[e]	−0.10[f]	+1.3[g]
	LDA	+1.80[h]		−6.80[i]	+0.56[j]	0.0[k]	
	GGA		+1.06[l], +1[l]		−0.80[m]	−0.03[n]	+0.87[o]
	GGA		+1.08[l], +1.15[p]				+1.20[q]
	LEED	+1.8[r]	+2.2 ± 1.3[s]	−2.1[t]	−0.7 ± 0.5[u]	+1.3 ± 1.3[v]	+1.0 ± 0.1[w]
	LEED	+1.9 ± 0.4[x]	+0.9 ± 0.5[y]	−4.9[z]	−0.3 ± 1.0[z1]	+2.4 ± 0.9[z2]	+1.0[s]
	LEED		+1.7 ± 0.3[z3]				
	LEED		+1.3 ± 0.8[z4]				
Δd_{23}	LDA[a]	+0.36 (−3.39)	+0.54 (−2.94)	+2.64 (−2.78)	−0.73 (−5.34)	−0.53 (−2.81)	−0.22 (−1.99)
(%)	PBE[b]	+0.24 (+0.23)	+0.54 (+0.24)	+2.82 (+1.91)	−0.65 (−0.14)	−0.41 (+2.49)	−0.29 (+2.83)
	LDA	+0.31[b], +0.50[c]		+2.80[d]	−0.64[e]		+0.3[g]
	LDA	+0.20[h]		+1.2[i]	−0.07[j]		
	GGA		−1.53[l],−2[l]		−0.58[m]	+0.08[n]	−0.50[q]
	GGA		−0.10[l],−0.05[p]				
	LEED	0.0[r]	+0.5 ± 0.7[z3]	+1.4[z]		−1.3 ± 1.3[v]	
	LEED	+0.8 ± 0.4[x]				+0.7 ± 0.9[z2]	
Δd_{34}	LDA[a]	−0.73 (−3.69)	+1.04 (−2.18)	+0.37 (−6.91)	−0.43 (−4.98)	−0.33 (−2.79)	−0.17 (−1.86)
(%)	PBE[b]	−0.72 (−0.73)	+1.06 (+0.94)	−0.51 (−1.90)	−0.24 (−0.06)	−0.22 (+2.24)	−0.21 (+2.77)
	LDA	+0.21[b], +0.10[c]			−0.26[e]		+0.5[g]
	LDA	−0.3[h]			+0.55[j]		
	GGA		−0.54[l], +0.05[l]		−0.15[m]	0.00[n]	
	GGA		+0.46[p]				
	LEED	0.0[r]		−1.1[z]		+2.2 ± 1.3[v]	
	LEED	−0.4 ± 0.4[x]				+0.7 ± 1.8[z2]	

The numbers in parentheses were obtained using the experimental lattice constant instead of the theoretical lattice constant. "+" and "−" indicate expansion and contraction of the interlayer spacings, respectively. $N_l = 7$ for Al(111), Cu(111), Pd(111), Pt(111) and 8 for Mg(0001) and Ti(0001).

[a] Present work using the FP-LAPW method.
[b] Ref. [45].
[c] Ref. [37].
[d] Ref. [39].
[e] Ref. [35].
[f] Ref. [7].
[g] Ref. [50].
[h] Ref. [44].
[i] Ref. [41].
[j] Ref. [48].
[k] Ref. [38].
[l] Ref. [46].
[m] Ref. [51].
[n] Ref. [49].
[o] Ref. [43].
[p] Ref. [11].
[q] Ref. [47].
[r] Ref. [33].
[s] Ref. [22].
[t] Ref. [20].
[u] Ref. [25].
[v] Ref. [26].
[w] Ref. [21].
[x] Ref. [29].
[y] Ref. [24].
[z] Ref. [32].
[z1] Ref. [23].
[z2] Ref. [30].
[z3] Ref. [28].
[z4] Ref. [31].

lattice constant is only 0.56% larger, so the interlayer relaxations do not deviate substantially (−0.44% versus −1.19%) when calculated at the theoretical or experimental lattice constants. For Pd(111), the experimental lattice

constant is about 1.0% greater compared to that obtained using the LDA, and 1.5% smaller compared to that obtained using the PBE. Thus, with the atoms relaxing to try and preserve the theoretical equilibrium volume, there is a contraction of the first interlayer spacing for the case of the LDA (−2.2%) and an expansion for the PBE (2.94%) when calculated at the experimental lattice constant, given that the relaxations obtained using the theoretical lattice constant are practically zero. The results for the other surfaces can be similarly understood. It is thus very important to use the theoretical lattice constant, and not simply the experimental value.

In the following, we will describe the interlayer spacings obtained using the LDA (and the theoretical equilibrium lattice constant), since the PBE predicts very similar results as mentioned above. For Mg(0001), we found a small expansion of +1.18% for the topmost interlayer spacing, which is in good agreement with LEED results, e.g., $\Delta d_{12} = +1.8\%$ [33] and $+1.9 \pm 0.4\%$ [29]. The experimentally determined interlayer spacings reported in Ref. [29] were obtained at temperature of 100 K, while in Ref. [33], they were extrapolated to zero temperature. Furthermore, we found an expansion of +0.36% and a contraction of −0.73% for the second and third interlayer spacings. Our results are in good agreement with the PPPW calculations reported in Refs. [37,44,45], except for the third interlayer spacing, which was reported to expand in Refs. [37,45].

For Al(111) there is an expansion of the first, second and third interlayer spacings of +1.35%, +0.54%, and +1.04%. PPPW calculations reported an expansion of the topmost layer by +1.05% and a contraction of −1.53% and −0.54% for the second and third interlayer spacings, respectively [46]. Recent FP-LAPW calculations performed by Da Silva [11] using a slab with seven layers (15 layers) found relaxations of +0.90% (+1.15%), −0.47% (−0.05%), and +0.46% (+0.46%) for the first, second, and third interlayer spacings, respectively, which differs from our results for the second interlayer spacing. The LEED intensity analyses find an expansion of the topmost interlayer spacing by $+2.2 \pm 1.3\%$ [22], $+0.9 \pm 0.5\%$ [24], $+1.7 \pm 0.3\%$ [28], and $1.3 \pm 0.8\%$ [31], while $0.5 \pm 0.7\%$ [28] was found for the second interlayer spacing. Therefore, there is good agreement between our results and LEED analyses, however, the sign of the relaxation of the second interlayer spacing obtained by LEED should be taken with caution due to the very small value and large (relative) error.

For Ti(0001), our calculations yield a contraction of the topmost interlayer spacing of −6.44%, while the second and third interlayer spacing expands by +2.64% and +0.37%, respectively. The contraction of the topmost interlayer spacing is in good agreement with PPPW calculations (−6.8%) [41], while LAPW calculations [39] predict a slightly greater first layer contraction (−7.7%). However, LEED analysis of the Ti(0001) surface predicts a contraction of only $-2.1 \pm 2.1\%$ [20]; significantly less than predicted theoretically. Recently, Teeter and Erskine studied the influence of hydrogen contamination on the interlayer spacings of Ti(0001) by LEED intensity analyses and electron-energy loss spectroscopy [32]. They reported that it is impossible to maintain a hydrogen-free Ti(0001) surface during the LEED measurements. A value of $-4.9 \pm 1\%$ was reported for the topmost interlayer spacing, which was obtained for between 13% and 23% of the hydrogen saturation coverage limit. They suggested that if Δd_{12} is linear with hydrogen coverage, the interlayer spacing of a hydrogen-free surface should be from 10% up to 20% greater than −4.9%, i.e., ≈ −6%, which is close to our theoretical calculations.

For Cu(111), there is a small contraction of the first, second, and third interlayer spacings by −1.25%, −0.46%, and −0.20%, respectively. The contraction of the topmost interlayer spacing is consistent with LEED intensity analyses, which obtained $-0.3 \pm 1.0\%$ [23] and $-0.7 \pm 0.5\%$ [25]. Our result for Δd_{12} is in good agreement with PPPW calculations reported in Ref. [35], but is in contrast to the PPPW calculations reported in Ref. [48], which found an expansion for the topmost interlayer spacing. Furthermore, our results are fully in accord with similar calculations performed by Da Silva et al. [51] using the FP-LAPW method.

For Pd(111), our results yield a very small contraction of the three outermost interlayer spacings. A LEED analysis reports an *expansion* of the topmost interlayer spacing, e.g., $+1.3 \pm 1.3\%$ [26], while a contraction and an expansion of the second and third interlayer spacings of $-1.3 \pm 1.3\%$ and $+2.2 \pm 1.3\%$ was reported [26], respectively. It can be noted that the expansion of the third interlayer spacing is larger than for the topmost interlayer spacing, which is not often seen in multilayer relaxations. The difference between theory and LEED might be due to the presence of hydrogen on the surface and in the subsurface region, in view of the easy adsorption of hydrogen atoms in bulk palladium and the resulting difficulty in keeping the Pd(111) surface free of hydrogen [26]. First-principles calculations using the same FP-LAPW method and same correlation functional [49] as used in the present work obtained a very similar small contraction of the first interlayer spacing (−0.03%), while for the second layer, a small expansion of 0.08% was obtained, in contrast to the small contraction obtained in the present work. From investigation of the potential energy surface related to the second interlayer spacing minimum by the authors of Ref. [49], it was found that it is very shallow.

For Pt(111), similar to the Mg(0001) and Al(111) surfaces, we find an expansion of the topmost interlayer spacing, i.e., the LDA result is +0.88%, which is in good agreement with LEED results, which found an expansion of $+1.0 \pm 1.3\%$ [22] and $+1.0 \pm 0.1\%$ [21]. The second and third layers contract slightly by 0.22% and 0.17%. DFT calculations, employing a linear combination of atomic orbitals, obtained an expansion of 0.87% [43] for the first interlayer spacing, in close agreement with our

result, while PPPW calculations within the GGA functional obtained that the first and second interlayer spacings expand and contract by +1.20% and −0.50%, respectively [47], also in good agreement with our results.

4. Conclusion

We calculated surface energies, work functions, and the interlayer relaxations of the close-packed Mg(0001), Al(111), Ti(0001), Cu(111), Pd(111), and Pt(111) surfaces employing the all-electron FP-LAPW method using the LDA and PBE functionals. All surface properties were calculated using the theoretical and experimental equilibrium lattice constants. The highly converged results obtained in the present work can be used as a reference or "benchmark" for other calculation approaches, e.g., to help in the construction of pseudopotentials, or for comparison with experimental results.

For Cu(111), the mentioned surface properties were studied as a function of the number of layers in the slab. From these calculations, we found that the surface energy, computed using Eq. (1) with slab and total energies obtained from separate DFT calculations, converges as a function of the number of layers in the slab, as expected, *provided* both calculations are carried out with the same high accuracy. In previous studies, such convergence was not obtained [12,14,13] which from our systematic study, we believe to be due to a lack of a sufficiently high accuracy with respect to the integrations of the bulk and surface Brillouin zones. We obtained a similar good convergence for the work function and multilayer relaxations.

Our results show that the LDA and PBE functionals predict very similar interlayer spacing relaxations for all the studied close-packed surfaces, provided the respective LDA and PBE equilibrium lattice constants are used. Therefore, in the study of the interlayer spacing relaxations, at least for the studied systems and tested functionals, the exchange–correlation functional does not play a significant role. However, the same is not true for the surface energy and work functions, which depends quite strongly on the exchange–correlation functional. The PBE in general predicts lower surface energies and smaller work functions as compared to the LDA. The experimental *trends*, however, are described correctly by both functionals. Furthermore, we found that both functionals predict very different interlayer relaxations if the experimental lattice constant is used, while, comparatively little difference is observed in the surface energies and work functions. We found good agreement between theoretical and experimental results for the bulk and surface properties, however, in some particular cases, discrepancies were found. For example, the experimental contraction of the topmost interlayer spacing of the Ti(0001) surface is almost three times larger than our theoretical result. This is thought to be due to hydrogen contamination.

Appendix A

The slab and bulk total energies used to compute the surface energies of Cu(111) plotted in Fig. 2 are listed in Table 4. Below, we test the affect that the error introduced due to the broadening parameter used in the Fermi–Dirac distribution function has on the surface properties.

The accuracy and the computational effort of first-principles calculations performed for periodic systems depends directly on the cutoff energy and integration of the BZ. Careful tests with respect to the cutoff energy and number of **k**-points in the BZ for the bulk and surface properties have been reported in Ref. [15]. Here, we focus just on the BZ integration. Commonly, two approaches are used to perform the integration: (i) the special **k**-points method with a broadening of the Fermi surface by the Fermi–Dirac

Table 4
Total energies of Cu(111) slabs, $E_{\mathrm{tot}}^{\mathrm{slab}}$, as obtained using the **k**-point sets of $(8\times8\times1)$ and $(16\times16\times1)$, which were used to calculate the surface energies according to: $\sigma = 1/2\left(E_{\mathrm{tot}}^{\mathrm{slab}} - N_{\mathrm{l}}E_{\mathrm{tot}}^{\mathrm{bulk}}\right)$

N_{l}	$E_{\mathrm{tot}}^{\mathrm{slab}}$; $(16\times16\times1)$		$E_{\mathrm{tot}}^{\mathrm{slab}}$; $(8\times8\times1)$	
	LDA	PBE	LDA	PBE
1	−3304.886551	−3310.005498	−3304.882540	−3310.001969
2	−6609.843529	−6620.060413	−6609.837166	−6620.054219
3	−9914.805616	−9930.120684	−9914.805238	−9930.119891
4	−13219.774737	−13240.187823	−13219.769038	−13240.181958
5	−16524.740734	−16550.251907	−16524.740343	−16550.250799
6	−19829.709071	−19860.318046	−19829.700196	−19860.309797
7	−23134.672660	−23170.380174	−23134.664074	−23170.372424
8	−26439.642232	−26480.447501	−26439.635347	−26480.441065
9	−29744.606648	−29790.510367	−29744.598594	−29790.503211
10	−33049.573588	−33100.576225	−33049.563732	−33100.567235
11	−36354.539425	−36410.640675	−36354.528916	−36410.630942
12	−39659.506925	−39720.706165	−39659.493695	−39720.693812

The three values of the bulk total energy per atom are: (i) $E_{\mathrm{tot}}^{\mathrm{bulk}} = -3304.966866$ Ry and −3310.065074 Ry for the **k**-point set of $(16\times16\times16)$ for the LDA and PBE, respectively; (ii) $E_{\mathrm{tot}}^{\mathrm{bulk}} = -3304.964146$ Ry and −3310.062791 Ry using the **k**-point set of $(8\times8\times8)$ for the LDA and PBE, respectively; (iii) from a linear fit using $N_{\mathrm{l}} = 3$ up to 12 for the slab calculations using the **k**-point set of $(8\times8\times1)$, $E_{\mathrm{tot}}^{\mathrm{fit}} = -3304.965446$ Ry and −3310.063874 Ry for the LDA and PBE, respectively.

Table 5
Interlayer spacing relaxations, Δd_{ij}, work function, Φ, and the surface energy, σ, of the Pd(1 1 1) surface calculated using different values for the broadening parameter, $k_B T_{elec}$, used in the integration of the surface BZ

$k_B T_{elec}$ (eV)	Δd_{12} (%)	Δd_{23} (%)	Φ (eV)	σ (eV/atom)	ΔE_{tot}^{slab} (eV)
0.30	−0.39	−0.15	5.55	0.77	0.23
0.20	−0.43	−0.51	5.59	0.77	0.11
0.11	−0.31	−0.83	5.63	0.77	0.03
0.05	−0.24	−0.88	5.65	0.77	0.01
0.01	−0.18	−0.92	5.68	0.78	0.00
TETRA	−0.18	−1.09	5.67	0.78	0.00

The relative error in the slab total energy, with respect to the total energy computed using the modified tetrahedron method, i.e., $\Delta E_{tot}^{slab} = E_{tot}^{slab}(\text{TETRA}) - E_{tot}^{slab}(k_B T_{elec})$, is also reported.
Note: TETRA indicates that these results were obtained using the modified tetrahedron method in the integration of the surface BZ using a $(16 \times 16 \times 1)$ **k**-point mesh.

distribution function [64] and (ii) the modified tetrahedron method [76]. The physical quantities obtained with the former scheme depends on the magnitude of the broadening parameter, $k_B T_{elec}$, while the latter scheme is exact in principle, but it requires a large number of **k**-points. k_B is the Boltzman constant and T_{elec} is the artificial electronic temperature.

The broadening of the Fermi surface by the Fermi–Dirac distribution function is an approximation used to reduce the number of necessary **k**-points and to avoid instabilities in the self-consistent procedure for metallic systems. However, this approach induces errors in the electron density due to the artificial occupation of the electronic states above the Fermi level, and hence, it introduces an error in the total energy. The total energy at zero electronic temperature is obtained by an extrapolation proposed in Ref. [66], i.e., $E_{tot}(T_{elec} = 0) \approx E_{tot}(T_{elec}) - \frac{1}{2} T_{elec} S(T_{elec})$, where $S(T_{elec})$ denotes the entropy associated with the occupation numbers of the electronic states. The expression for $S(T_{elec})$ is obtained for a free-electron gas system. Errors in forces due to the broadening parameter were discussed in Ref. [65] and we note a too large broadening parameter might affect the interlayer relaxations.

To test the accuracy of our calculations with respect to the broadening parameter, we choose the Pd(1 1 1) surface as a test case, which has a large density of states at the Fermi level. Therefore this system should be particularly sensitive to the broadening parameter. The calculations are performed for different values i.e., $k_B T_{elec} = 0.01$, 0.05, 0.11, 0.20, and 0.30 eV, while 30 **k**-points are used in the integration of the surface BZ, i.e., a $(16 \times 16 \times 1)$ **k**-point mesh. We use the LDA functional and a slab of five layers, which is sufficient since we are only interested in *changes* in the surface properties as a function of the broadening parameter. Calculations are also performed using the modified tetrahedron method for reference [a $(16 \times 16 \times 1)$ **k**-point mesh was also used]. The results are summarized in Table 5.

Broadening parameters in the range of 0.01–0.30 eV are found not play a critical role for the surface energy, while the work function is only slightly changed, i.e., it systematically decreases with increasing $k_B T_{elec}$. However, the interlayer spacings change significantly, as can be seen in Table 5. The relative error in the slab total energy with respect to the total energy computed using the modified tetrahedron method, i.e., $\Delta E_{tot}^{slab} = E_{tot}^{slab}(\text{TETRA}) - E_{tot}^{slab}(k_B T_{elec})$, increases with increase of the broadening parameter. For example, $\Delta E_{tot}^{slab} = 0.01$ eV and 0.23 eV for $k_B T_{elec} =$ 0.05 eV and 0.30 eV, respectively. Thus, the correction proposed in Ref. [66] does not adequately correct the total energy for large values of the broadening parameter. Therefore, the constant values of the surface energy as a function of the broadening parameter is due to error cancellation between the slab and bulk total energies used in Eq. (1) to compute the surface energy.

The slight changes in the work function are mainly due to changes in the Fermi level. The interlayer spacings clearly depend on the broadening parameter as mentioned above. For example, $\Delta d_{12} = -0.18\%$ and -0.39% for $k_B T_{elec} = 0.01$ eV and 0.30 eV, respectively, however, the largest change is obtained for the second interlayer spacing, e.g., $\Delta d_{23} = -0.92\%$ and -0.15% for $k_B T_{elec} = 0.01$ eV and 0.30 eV, respectively. Thus, the errors are not the same for all interlayer spacings. The surface properties calculated using $k_B T_{elec} = 0.01$ eV are almost the same as those computed using the modified tetrahedron method, which shows that by systematically decreasing the broadening parameter we can obtain highly accurate results; however, using small values for the broadening parameter introduces instabilities in the self-consistent procedure. From the tests reported in the present appendix, a value of 0.05 eV for the broadening parameter was chosen to perform all our surface calculations as it yields a balance between good accuracy and stability.

References

[1] M.-C. Desjonquères, D. Spanjaard, Concepts in Surface Science, Springer, 1995.
[2] M. Scheffler, C. Stampfl, Theory of adsorption on metal substrates, in: Electronic Structure, in: K. Horn, M. Scheffler (Eds.), Handbook of Surface Science, vol. 2, Elsevier, Amsterdam, 1999, p. 286.
[3] W.R. Tyson, W.A. Miller, Surf. Sci. 62 (1977) 267.
[4] F.R. De Boer, R. Boom, W.C.M. Mattens, A.R. Miedema, A.K. Niessen, Cohesion in Metals, North-Holland, Amsterdam, 1988.

[5] H.P. Bonzel, Phys. Rep. 385 (2003) 1.
[6] O. Pierre-Louis, J.-J. Métois, Phys. Rev. Lett. 93 (2004) 165901.
[7] M. Methfessel, D. Hennig, M. Scheffler, Phys. Rev. B 46 (1992) 4816; M. Methfessel, D. Hennig, M. Scheffler, Appl. Phys. A 55 (1992) 442.
[8] H.L. Skriver, N.M. Rosengaard, Phys. Rev. B 46 (1992) 7157.
[9] L. Vitos, A.V. Ruban, H.L. Skriver, J. Kollár, Surf. Sci. 411 (1998) 186.
[10] D.K. Yu, M. Scheffler, Phys. Rev. B 70 (2004) 155417.
[11] J.L.F. Da Silva, Phys. Rev. B 71 (2005) 195416.
[12] J.C. Boettger, Phys. Rev. B 49 (1994) 16798.
[13] J.C. Boettger, J.R. Smith, U. Bierkenheuer, N. Rösch, S.B. Trickey, J.R. Sabin, S.P. Apell, J. Phys. Condens. Matter 10 (1998) 893, and references therein.
[14] V. Fiorentini, M. Methfessel, J. Phys. Condens. Matter 8 (1996) 6525.
[15] J.L.F. Da Silva, The nature and behavior of rare-gas atoms on metal surfaces, Ph.D. Thesis, Technical University Berlin, Berlin, Germany, 2002. Available from: <http://edocs.tu-berlin.de/diss/2002/dasilva_juarez.htm> or <http://www.fhi-berlin.mpg.de/th/pub02.html>.
[16] J.L.F. Da Silva, C. Stampfl, M. Scheffler, Phys. Rev. Lett. 90 (2003) 66104.
[17] J.L.F. Da Silva, C. Stampfl, M. Scheffler, Phys. Rev. B 72 (2005) 075424.
[18] J. Hölzl, F.K. Schulte, H. Wagner, Work function of metals, in: Solid Surface Physics, Springer Tracts Modern Physics, vol. 85, Springer, Berlin, Heidelberg, 1979.
[19] P. Zeppenfeld, in: Physics of Covered Solid Surfaces, Landolt-Börnstein, New Series, Group III, vol. 42: Numerical Data and Functional Relationships in Science and Technology, Subvol. A: Adsorbed Layers on Surfaces, Springer-Verlag, Berlin, 2001, p. 67.
[20] H.D. Shih, F. Jona, D.W. Jepsen, P.M. Marcus, J. Phys. C 9 (1976) 1405.
[21] D.L. Adams, H.B. Nielsen, M.A. Van Hove, Phys. Rev. B 20 (1979) 4789.
[22] F. Jona, D. Sondericker, P.M. Marcus, J. Phys. C 13 (1980) L155.
[23] S.P. Tear, K. Röll, M. Prutton, J. Phys. C: Solid State Phys. 14 (1981) 3297.
[24] H.B. Nielsen, D.L. Adams, J. Phys. C 15 (1982) 615.
[25] S.Å. Lindgren, L. Walldén, J. Rundgren, P. Westrin, Phys. Rev. B 29 (1984) 576.
[26] H. Ohtani, M.A. Van Hove, G.A. Somarjai, Surf. Sci. 187 (1987) 372.
[27] F. Jona, P.M. Marcus, in: J.J. Van der Veen, M.A. Van Hove (Eds.), The Structure of Surfaces II, Springer Series in Surface Sciences, vol. 11, Springer-Verlag, Berlin, 1988, p. 90.
[28] J.R. Noonan, H.L. Davis, J. Vac. Sci. Technol. A 8 (1990) 2671.
[29] P.T. Sprunger, K. Pohl, H.L. Davis, E.W. Plummer, Surf. Sci. 297 (1993) L48.
[30] M.E. Grillo, C. Stampfl, W. Berndt, Surf. Sci. 317 (1994) 84.
[31] C. Stampfl, M. Scheffler, H. Over, J. Burchhardt, M. Nielsen, D.L. Adams, W. Moritz, Phys. Rev. B 49 (1994) 4959.
[32] G. Teeter, J.L. Erskine, Phys. Rev. B 61 (2000) 13929.
[33] Ismail, Ph. Hofmann, A.P. Baddorf, E.W. Plummer, Phys. Rev. B 66 (2002) 245414.
[34] P.J. Feibelman, D.R. Hamann, Surf. Sci. 234 (1990) 377.
[35] Th. Rodach, K.-P. Bohnen, K.M. Ho, Surf. Sci. 286 (1993) 66.
[36] H.M. Polatoglou, M. Methfessel, M. Scheffler, Phys. Rev. B 48 (1993) 1877.
[37] A.F. Wright, P.J. Feibelman, S.R. Atlas, Surf. Sci. 302 (1994) 215.
[38] W. Dong, G. Kresse, J. Fruthmüller, J. Hafner, Phys. Rev. B 54 (1996) 2157.
[39] P.J. Feibelman, Phys. Rev. B 53 (1996) 13740.
[40] P.J. Feibelman, Surf. Sci. 360 (1996) 297.
[41] J.-H. Cho, K. Terakura, Phys. Rev. B 56 (1997) 9282.
[42] H.W.L. Alvez, J.L.A. Alves, J.L.F. Da Silva, J.R. Leite, R.A. Nogueira, Mater. Sci. Eng. B Solid 59 (1999) 258.
[43] A. Kokalj, M. Causà, J. Phys. Condens. Matter 11 (1999) 7463.
[44] P. Staikov, T. Rahman, Phys. Rev. B 60 (1999) 15613.
[45] E. Wachowicz, A. Kiejana, Surf. Sci. 116 (2000) 17.
[46] A. Kiejana, B.J. Lundqvist, Phys. Rev. B 63 (2001) 85405.
[47] S. Moré, A.P. Seitsonen, W. Berndt, A.M. Bradshaw, Phys. Rev. B 63 (2001) 75406.
[48] J.C. Zheng, H.Q. Wang, A.T.S. Wee, H.A. Huan, Surf. Rev. Lett. 8 (2001) 541.
[49] M. Todorova, K. Reuter, M. Scheffler, J. Phys. Chem. B 108 (2004) 14477.
[50] S. Baud, C. Ramseyer, G. Bihlmayer, S. Blügel, C. Barreteau, M.C. Desjonquéres, D. Spanjaard, N. Bernstein, Phys. Rev. B 70 (2004) 235423.
[51] J.L.F. Da Silva, K. Schroeder, S. Blügel, Phys. Rev. B 69 (2004) 245411.
[52] J.L.F. Da Silva, K. Schroeder, S. Blügel, Phys. Rev. B 70 (2004) 245432.
[53] J.L.F. Da Silva, K. Schroeder, S. Blügel, Phys. Rev. B 72 (2005) 033405.
[54] P. Hohenberg, W. Kohn, Phys. Rev. 136 (1964) B864.
[55] W. Kohn, L.J. Sham, Phys. Rev. 140 (1965) A1133.
[56] J.P. Perdew, Y. Wang, Phys. Rev. B 45 (1992) 13244.
[57] J.P. Perdew, J.A. Chevary, S.H. Vosko, K.A. Jackson, M.R. Pederson, D.J. Singh, C. Flolhais, Phys. Rev. B 46 (1992) 6671.
[58] J.P. Perdew, S. Burke, M. Ernzerhof, Phys. Rev. Lett. 77 (1996) 3865.
[59] D.J. Singh, Plane Waves, Pseudopotentials and LAPW Method, Kluwer Academic Publishers, Boston, Dordrecht, London, 1994.
[60] P. Blaha, K. Schwarz, J. Luitz, WIEN97, A full-potential linearized augmented plane wave package for calculating crystal properties, Karlheinz Schwarz, Techn. Univ. Wien, Vienna, 1999. ISBN 3-9501031-0-4, Updated version of P. Blaha, K. Schwarz, P. Sorantin, S.B. Trickey, Comput. Phys. Commun. 59 (1990) 399.
[61] M. Petersen, F. Wagner, L. Hufnagel, M. Scheffler, P. Blaha, K. Schwarz, Comput. Phys. Commun. 126 (2000) 294.
[62] R. Dohmen, J. Pichlmeier, M. Petersen, F. Wagner, M. Scheffler, Comput. Sci. Eng. 3 (2001) 18.
[63] B. Kohler, S. Wilke, M. Scheffler, R. Kouba, C. Ambrosch-Draxl, Comput. Phys. Commun. 94 (1996) 31.
[64] H.J. Monkhorst, J.D. Pack, Phys. Rev. B 13 (1976) 5188.
[65] F. Wagner, Th. Laloyaux, M. Scheffler, Phys. Rev. B 57 (1998) 2102.
[66] M.G. Gillan, J. Phys. Condens. Matter 1 (1989) 689.
[67] F.D. Murnaghan, Proc. Natl. Acad. Sci. USA 50 (1944) 697, The Murnaghan's equation of state is given by the following equation: $E_{\mathrm{tot}}(V) = \frac{B_0 V_0}{B_0'(B_0'-1)}\left(\frac{V}{V_0}\right)^{(1-B_0')} + \frac{B_0 V}{B_0'} - \frac{B_0 V_0}{(B_0'-1)} + E_{\mathrm{tot}}(V_0)$, where V, V_0, B_0, and B_0' are the volume, volume at zero pressure, bulk modulus calculated at zero pressure, and derivative of the bulk modulus with respect pressure calculated at zero pressure, respectively. Hence, using the Murnaghan's equation, we can obtain the bulk modulus as a function of the pressure $[B(p) = B_0 + B_0' p]$ and the bulk modulus as a function of the volume $\left[B(V) = \left(V\frac{\mathrm{d}^2 E_{\mathrm{tot}}(V)}{\mathrm{d}V^2}\right) = B_0\left(\frac{V_0}{V}\right)^{B_0'}\right]$.
[68] C. Kittel, in: Introduction to Solid State Physics, seventh ed., John Wiley & Sons, Inc., 1996.
[69] M. Fuchs, M. Bockstedte, E. Pehlke, M. Scheffler, Phys. Rev. B 57 (1998) 2134.
[70] M. Fuchs, L.L.F. Da Silva, C. Stampfl, J. Neugbauer, M. Scheffler, Phys. Rev. B 65 (2002) 245212.
[71] A. Khein, D.J. Singh, C.J. Umrigar, Phys. Rev. B 51 (1995) 4105.
[72] P.H.T. Philipsen, E.J. Baerends, Phys. Rev. B 54 (1996) 5326.
[73] G.N. Derry, Z. Ji-Zhong, Phys. Rev. 39 (1989) 1940.
[74] R. Gomer, Acc. Chem. Res. 29 (1996) 284.
[75] T. Fauster, W. Steinman, in: P. Halevi (Ed.), Electromagnetic Waves: Recent developments in Research, Elsevier, Amsterdam, 1995.
[76] P.E. Blöchl, O. Jepsen, O.K. Andersen, Phys. Rev. B 49 (1994) 16223.